surrounds the nearside basins. These last deposits may reflect a separate rock type that is mafic in composition, or may merely reflect numerous, unresolved small-area basalt deposits that dot these regions.

The overall correlation is sufficient to suggest that the measured thermal and fast neutron fluxes, on spatial scales on the order of 200 km (fast neutrons) to 450 km (thermal neutrons) diameter areas (for an LP altitude of 100 km), reveal a smooth transition from a predominantly mafic composition at low altitudes to a predominantly feldspathic composition at high altitudes. The more mafic deposits result from excavation of highlands material by the impacts that created all of the big basins such as SPA, thereby exposing material from the lower crust and perhaps the upper mantle (*13*), whereas the feldspathic composition reflects the top of the crust that is exposed in the highlands.

References and Notes

1. D. M. Drake, W. C. Feldman, B. M. Jakosky, *J. Geophys. Res.* **93**, 6353 (1988).
2. J. Masarik and R. C. Reedy, *ibid.* **101**, 18891 (1996).
3. R. C. Reedy *et al.*, *Meteor. Planet. Sci.* **33** (no. 4, suppl.), A127.
4. W. C. Feldman *et al.*, *J. Geophys. Res.* **102**, 25565 (1997).
5. R. E. Lingenfelter, E. H. Canfield, V. E. Hampel, *Earth Planet. Sci. Lett.* **16**, 355 (1972).
6. W. C. Feldman, R. C. Reedy, D. S. McKay, *Geophys. Res. Lett.* **18**, 2157 (1991).
7. R. C. Elphic *et al.*, *Science* **281**, 1493 (1998).
8. W. C. Feldman *et al.*, *Nucl. Instrum. Methods Phys. Res. A*, in press.
9. A. B. Binder, *Science* **281**, 1475 (1998).
10. W. C. Feldman, D. M. Drake, R. D. O'Dell, F. W. Brinkley Jr., R. C. Anderson, *J. Geophys. Res.* **94**, 513 (1989).
11. W. C. Feldman and D. M. Drake, *Nucl. Instrum. Methods Phys. Res.* **A245**, 182 (1986).
12. D. E. Smith, M. T. Zuber, G. A. Neumann, F. G. Lemoine, *J. Geophys. Res.* **102**, 1591 (1997).
13. M. A. Wieczorek and R. J. Phillips, *ibid.* **103**, 1715 (1998).
14. W. C. Feldman *et al.*, *Science* **281**, 1496 (1998).
15. R. C. Byrd and W. T. Urban, *LANL Doc. LA-12833-MS* (1994).
16. P. G. Lucey, D. T. Blewett, B. R. Hawke, *J. Geophys. Res.* **103**, 3679 (1998).
17. L. Haskin and P. Warren, in *Lunar Sourcebook, a User's Guide to the Moon*, G. H. Heiken, D. T. Vaniman, B. M. French, Eds. (Cambridge Univ. Press, Cambridge, 1991), pp. 357–474.
18. R. E. Alcouffe *et al.*, *LANL Manual LA-7369-M*, rev. 2 (1995).
19. P. G. Lucey, P. D. Spudis, M. Zuber, D. Smith, E. Malaret, *Science* **266**, 1855 (1994).

20. Supported in part by Lockheed Martin under contract to NASA and conducted under the auspices of the U.S. Department of Energy.

13 July 1998; accepted 10 August 1998

Lunar Fe and Ti Abundances: Comparison of Lunar Prospector and Clementine Data

R. C. Elphic,* D. J. Lawrence, W. C. Feldman, B. L. Barraclough, S. Maurice, A. B. Binder, P. G. Lucey

The Lunar Prospector neutron spectrometer data correlate well with iron and titanium abundances obtained through analysis of Clementine spectral reflectance data. With the iron and titanium dependence removed, the neutron spectrometer data also reveal regions with enhanced amounts of gadolinium and samarium, incompatible rare earth elements that are enriched in the final phases of magma crystallization. These regions are found mainly around the ramparts of the Imbrium impact basin but not around the other basins, including the much larger and deeper South Pole–Aitken basin. This result confirms the compositional uniqueness of the surface and interior of the Imbrium region.

The surface of the moon provides a record of the early evolution of the Earth-moon system through the period of heavy bombardment ~4 billion years ago. In contrast, most terrestrial rocks are much younger. Throughout the moon's history large impacts have excavated material from the lower crust (and possibly the mafic upper mantle) and deposited it on the surface. Basaltic volcanism during and after the heavy bombardment epoch flooded some impact basins with material derived from partial melting of the upper mantle and lower crust. Study of these materials thus provides a window into the moon's interior. Whereas most of our understanding of lunar composition is derived primarily from returned Apollo and Luna samples, the question remains to what extent these samples are representative of the whole moon.

A major step toward a global assessment of lunar surface chemistry was provided by analysis of spectral reflectance data returned by the Clementine mission. Comparison of the spectral reflectance properties and chemical compositions of lunar soils returned by the Apollo and Luna missions, and remote measurement of the spectral properties of the Apollo and Luna sample collection sites by Clementine, led to the development of algorithms that derive the abundance of FeO and TiO_2 from spectral properties of lunar soils and surface units with 1 to 2 weight % accuracy. By applying these algorithms to Clementine global imaging, it has been possible to infer the quantitative abundance of FeO and TiO_2 within $\pm 80°$ latitude (*1–4*) at resolutions approaching 100 m. The approach was calibrated with lunar samples returned from a relatively small area of the lunar nearside, and it is possible that areas distant from the landing sites, such as the farside, might have different mineralogies. Thus, the inferred FeO and TiO_2 values might be spurious there (*5*). Here, we test the validity of the Clementine spectral reflectance (CSR) method with independent analyses of Fe and Ti, using data from the Lunar Prospector (LP) neutron spectrometer (*6, 7*).

The neutron spectrometer measures neutrons at thermal (0.001 to 0.3 eV), epithermal (0.3 eV to 500 keV), and fast (500 keV to 8 MeV) energies. Lunar neutrons are created by the interaction of galactic cosmic rays with the nuclei in the lunar regolith; they are produced in the fast regime at high energies as a direct result of spallation. These neutrons inelastically scatter off of other nuclei in the soil, losing energy as they pass through the epithermal regime. When their energies approach that corresponding to the temperature of the ambient regolith (thermal regime), the neutrons are captured by nuclei that have large cross sections for thermal neutron absorption (*8*). Iron and titanium are the most abundant elements with large absorption cross sections; consequently, they have considerable influence on thermal neutron fluxes. In addition, Fe and Ti evidently produce more fast neutrons than elements with lower atomic numbers (*9*). Consequently, when LP is above the Fe- and Ti-rich maria, the neutron spectrometer detects a higher fast neutron flux and a lower thermal neutron flux (*6, 7*). We report on neutron data acquired during the first 6 months of the LP mapping mission, beginning 16 January 1998.

The neutron spectrometer measures the net production of fast neutrons from the elements in the regolith below LP and the net

R. C. Elphic, D. J. Lawrence, W. C. Feldman, B. L. Barraclough, Space and Atmospheric Sciences, MS D466, Los Alamos National Laboratory, Los Alamos, NM 87545, USA. S. Maurice, Observatoire Midi-Pyrénées, 31400 Toulouse, France. A. B. Binder, Lunar Research Institute, Gilroy, CA 95020, USA. P. G. Lucey, Hawai'i Institute of Geophysics and Planetology, University of Hawai'i, Honolulu, HI 96822, USA.

*To whom correspondence should be addressed. E-mail: relphic@lanl.gov

flux of thermal neutrons resulting from production, moderation, and absorption due to all species. Consequently, it is not possible to directly infer the abundances of Fe and Ti separately with neutron spectrometer data alone. Instead, we use the most recently generated CSR Fe and Ti maps from (*4*) to predict how much neutron production and absorption should be seen and compare that prediction to what was actually observed.

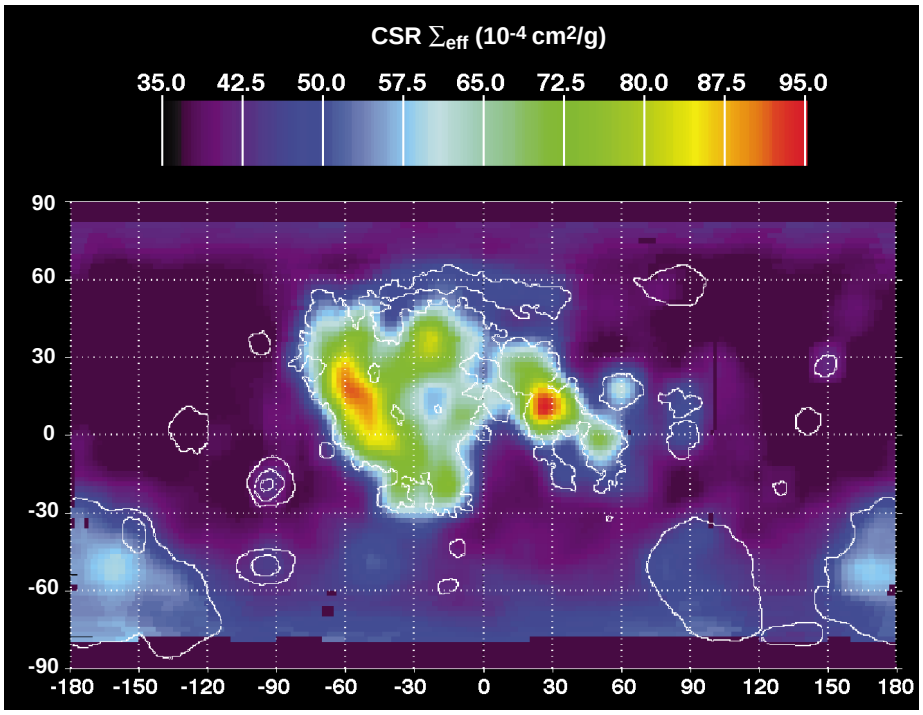

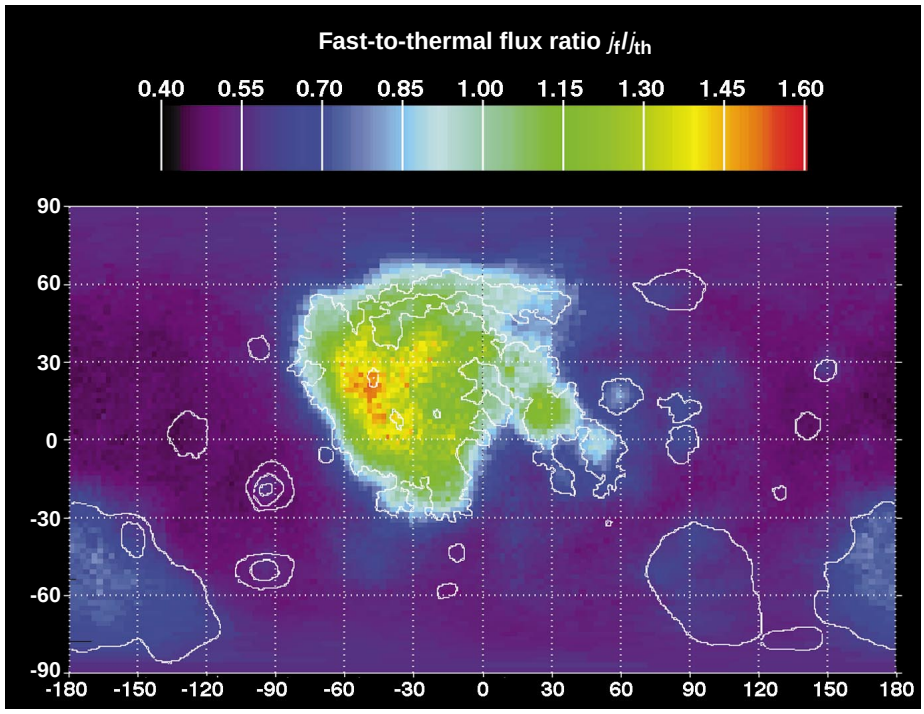

Fig. 1 (top). Macroscopic absorption cross section Σ_{eff} as determined from CSR Fe and Ti abundances. The original 0.25° by 0.25° map was smoothed with the thermal neutron response function but is binned in 2° by 2° (~60 km by 60 km) pixels. Local highs in Σ_{eff} can be seen over the nearside maria and over the South Pole–Aitken basin, where Fe and Ti concentrations are higher than the surrounding highlands. **Fig. 2 (bottom)**. Ratio of the LP fast-to-thermal neutron count rates, j_f/j_{th}. This quantity should be directly related to the abundance of thermal neutron absorbers in the regolith. Highs similar to Fig. 1 are found over the maria and the South Pole–Aitken basin. Data from the first 6 months of LP mapping are shown.

Any differences must be due to either a surplus or a lack of neutron absorbers, that is, Fe or Ti in unseen mineral phases, or other possible neutron absorbers.

To compare the CSR maps [which have a surface resolution of 0.25° (7.5 km)] to the neutron observations from LP, we convolved the maps with the effective surface response functions of the neutron detector. For thermal neutrons, the relevant surface area has an effective footprint diameter of about 700 km for a 100-km orbit. The fast neutron footprint is smaller, 350 km in diameter.

The fast neutron flux should correlate with the Fe and Ti content in the regolith. The maps shown in (*7*) are in qualitative agreement with the published CSR Fe and Ti abundances (*4*). Overall, the correlation coefficient between the fast neutron count rate and the CSR Fe+Ti weight % values is 0.811. For a more restricted latitude range (where possible problems associated with lighting in the CSR data are reduced), ±60°, the correlation improves to 0.887. For a region including the eastern nearside maria and some farside highlands (40° to 180°E longitude, ±60° latitude), the correlation coefficient is 0.930, whereas for the nearside maria region alone (90°W to 90°E longitude, −30° to 60° latitude), it is 0.941.

LP detected a low flux of thermal neutrons over the maria and South Pole–Aitken basin (*7*), indicative of the presence of high concentrations of Fe and Ti. The net thermal neutron absorption in a given volume of regolith is related to the macroscopic absorption cross section

$$\Sigma_{eff} = \sum_i \sigma_{ai} f_i N_A / A_i \qquad (1)$$

where f_i, σ_{ai}, and A_i are the weight fraction, thermal neutron absorption cross section, and atomic mass of element i, respectively, and N_A is Avogadro's number. Table 1 shows the contribution of the various elements to the total macroscopic absorption cross section for three bulk regolith compositions: an Apollo 11 high-Ti mare soil, an Apollo 16 low-Fe highlands soil, and an Apollo 14 KREEP basalt (KREEP is a component of some lunar rocks with a composition enriched in potassium, K, rare earth elements, REE, and phosphorus, P). Fe and Ti are the biggest contributors to absorption in the mare soil; Fe is also the chief absorber (despite its low abundance) in the highlands soil, but Ca is almost as important. Silicon, Al, and the other major elements play a lesser, but not negligible, role in thermal neutron absorption.

Because Ca abundance is so variable on the moon, we must include its effects in our calculations. We make use of an observed inverse correlation between CaO and FeO

in lunar samples to do this (*10*). In samples with very low FeO abundances, CaO reaches about 20% by weight; as FeO approaches about 12%, CaO abundance drops linearly to about 10% and stays at about that level in materials with higher FeO abundances. We assume that the net absorption due to Si, Al, and other major elements is approximately constant at 18×10^{-4} cm^2/g.

Certain REEs have anomalously high cross sections for absorption of thermal neutrons because of nuclear resonances (*11*). Consequently, the effects of these rare earth elements can be disproportionate to their low chemical abundances. Gadolinium and Sm, in particular, can significantly affect Σ_{eff} in regions where they are abundant (>5 μg/g; see Table 1). Gadolinium and Sm are most abundant in KREEP, along with other incompatible elements such as Th, K, and U. These elements are enriched in the final phases of magma crystallization, and for this reason KREEP is thought to be derived from the lower crust. In the Apollo 14 KREEP basalts, the Gd and Sm contribution to neutron absorption is comparable with the total from all other elements and increases Σ_{eff} from 50.8×10^{-4} to 93.2×10^{-4} cm^2/g (*12*). The contributions of Sm and Gd to the Apollo 11 mare and Apollo 16 highlands Σ_{eff} values are about 10 and 13%, respectively (Table 1). We have not included the effects of Gd and Sm in our estimates of Σ_{eff} based on CSR-derived values of Fe and Ti abundances.

Simulations of neutron transport in lunar and martian regoliths have shown that the ratio of the fluxes of fast to thermal neutrons j_f/j_{th} is linearly related to Σ_{eff} (*12*). This is what would be expected: the more neutron absorbers in the regolith, the fewer the number of thermal neutrons observed per fast neutron created. Thus, j_f/j_{th} is the neutron measurement proxy that directly relates to the macroscopic absorption cross section Σ_{eff}.

Table 1. Contributions to Σ_{eff}, thermal neutron absorption. Ap, Apollo mission.

Compound	σ_a (b)*	$\sigma_a f N_A/A$ ($\times 10^{-4}$ cm^2/g)		
		Ap 11	Ap 16	Ap 14
SiO_2	0.16	6.84	7.29	8.59
TiO_2	5.8	32.30	1.75	7.29
Al_2O_3	0.23	1.97	3.64	2.05
FeO	2.53	32.36	11.85	23.15
MnO	13.2	2.24	1.12	2.17
MgO	0.06	0.73	0.59	0.56
CaO	0.46	5.54	7.17	4.50
Na_2O	0.51	0.29	0.29	0.40
K_2O	2.07	0.13	0.13	1.67
Sm	7,900	2.72	1.58	12.66
Gd	14,900	5.99	3.42	29.68
Total Σ_{eff}		91.40	38.97	88.34

*b, 10^{-28} m^2 per nucleus.

The macroscopic absorption cross section Σ_{eff} inferred from the CSR Fe and Ti results (Fig. 1) is high over western Oceanus Procellarum (50°W 15°N), Mare Imbrium (25°W 35°N), and Mare Tranquillitatis (25°E 10°N). The value of Σ_{eff} is also high in the South Pole–Aitken basin mainly because of the basin's high Fe content. The ratio of the fast to thermal neutron fluxes, j_f/j_{th}, as observed by LP, shows similar patterns but also some differences, particularly around the periphery of Mare Imbrium (Fig. 2). To compare these two data sets, we plot the neutron flux ratio j_f/j_{th} versus the inferred CSR macroscopic absorption cross section Σ_{eff} (Fig. 3). The observed absorption of thermal neutrons is often greater than would be expected on the basis of CSR Fe, Ti, and Ca.

The overall global correlation between Σ_{eff} calculated with the CSR Fe and Ti values and the proxy for macroscopic absorption coefficient, j_f/j_{th}, is 0.849. By restricting the latitude range to ±60° (black points in Fig. 3), the correlation improves to 0.903. A still more limited region covering the eastern maria and some farside highlands, 20°E to 180°E longitude and ±30° latitude (red points in Fig. 3), yields a correlation coefficient of 0.978. Thus, our calculated values of Σ_{eff} based on CSR Fe and Ti abundances correlate well with j_f/j_{th} in

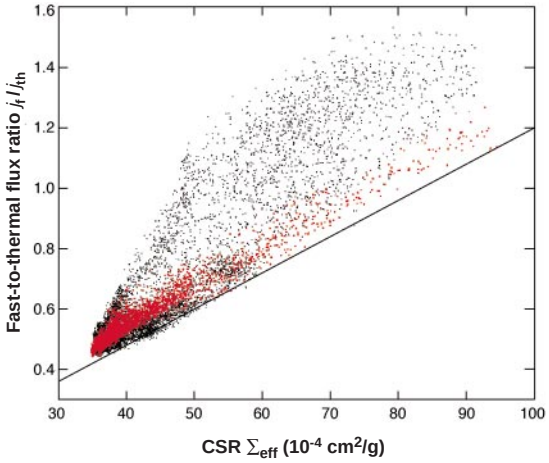

Fig. 3. Fast-to-thermal neutron count rate ratio j_f/j_{th} plotted versus CSR-derived Σ_{eff} for data from ±60° latitudes (black points). Red points represent data from a more restricted region (see text). The solid line is an ideal linear relation that would be expected if Fe, Ti, and Ca are the most important absorbing species. Flux ratio values to the left of this line indicate that the calculated values of Σ_{eff} based on CSR data are too low, and other neutron absorbers are present.

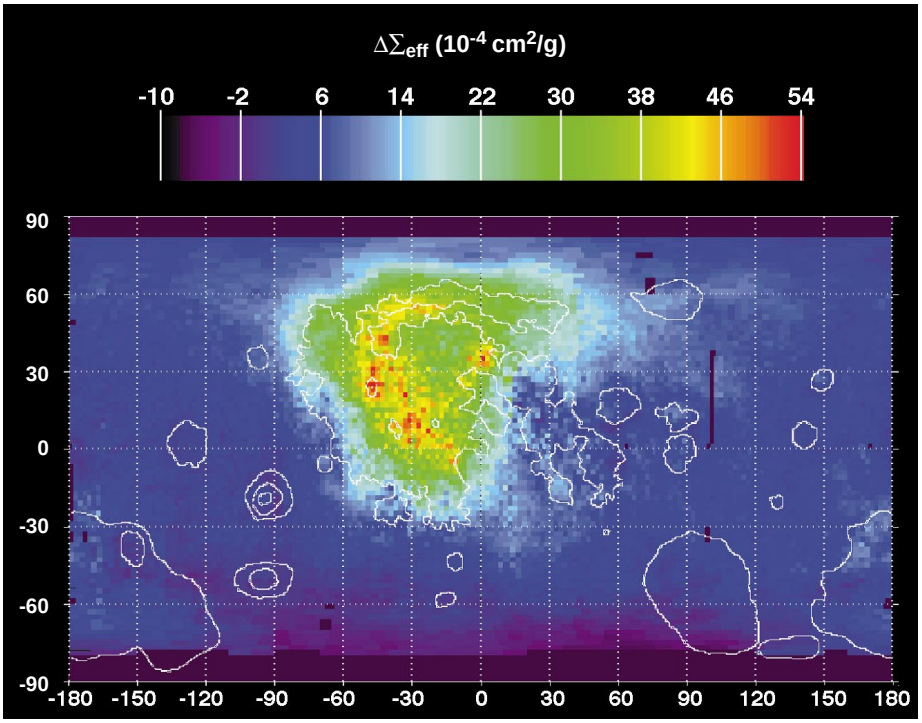

Fig. 4. Map of $\Delta\Sigma_{eff}$, a measure of thermal neutron absorbers in addition to Fe, Ti, and other major elements implied by CSR-derived abundances. The greatest values of $\Delta\Sigma_{eff}$ are found surrounding the Imbrium basin, approximately colocated with regions rich in KREEP.

some regions but not as well in others.

A map of the difference $\Delta\Sigma_{eff}$ between this linear relation and the calculated Σ_{eff} points (Fig. 3) reflects the implied abundance of neutron absorbers other than Fe and Ti (Fig. 4). The highest values are found over the rim of the Imbrium basin, including the Apennine mountains in the east up through the Alps, across to the Jura mountains in the west, down through the Aristarchus plateau and through the Fra Mauro formation to the south. LP gamma-ray spectrometer maps show that these regions also have high Th and K concentrations (*13*). This similarity implies that the absorbing species are affiliated with the incompatible elements found in KREEP; the correlation coefficient between the gamma-ray spectrometer Th data (*13*) and $\Delta\Sigma_{eff}$ is 0.93. The values of $\Delta\Sigma_{eff}$ are consistent with the range (10×10^{-4} to 42×10^{-4} cm^2/g) of Gd and Sm contributions listed in Table 1. The K in KREEP plays only a very minor role in Σ_{eff} (Table 1). Therefore, we conclude that $\Delta\Sigma_{eff}$ reflects primarily the concentration of Gd and Sm and, thus, is a tracer for KREEP.

The estimated thermal neutron macroscopic absorption coefficient that would be expected on the basis of concentrations of Fe and Ti derived from CSR data, coupled with an estimate of Ca concentrations, is in reasonable agreement with the LP neutron spectrometer results. Discrepancies arise in regions that have significant levels of KREEP, where Gd and Sm are major thermal neutron absorbers. Thus, the CSR method appears to be a reliable technique for obtaining FeO and TiO_2 abundances moonwide. The inferred KREEP-rich regions form a ring around the Imbrium impact site and are directly related to either excavation of this lower crustal chemistry or to volcanism that extruded KREEP-rich lava on the surface. On the other hand, the much larger, deeper South Pole–Aitken impact basin shows little KREEP enhancement (*14*). This result appears to confirm the uniqueness of the Imbrium lower crustal chemistry and suggests that the moon may have considerable regional compositional heterogeneity at depth.

References and Notes

1. P. G. Lucey, G. J. Taylor, E. Malaret, *Science* **268**, 1150 (1995).
2. P. G. Lucey, D. T. Blewett, J. R. Johnson, G. J. Taylor, B. R. Hawke, *Lunar Planet Sci.* **XXVII**, 781 (1996).
3. D. T. Blewett, P. G. Lucey, B. R. Hawke, B. L. Jolliff, *J. Geophys. Res.* **102**, 16319 (1997).
4. P. G. Lucey, D. T. Blewett, B. R. Hawke, *ibid.* **103**, 3679 (1998).
5. P. E. Clark and A. Basu, *Proc. Lunar Planet. Sci. Conf.* **29**, 1501 (1998). Olivine is the likeliest mineral to be underrepresented in the results from analysis of spectral data.
6. W. C. Feldman *et al.*, *Science,* **281** 1496 (1998).
7. W. C. Feldman *et al.*, *ibid.,* p. 1489 (1998).
8. D. M. Drake, W. C. Feldman, B. M. Jakosky, *J. Geophys. Res.* **93**, 6353 (1988).
9. R. C. Reedy *et al.*, *Meteorit. Planet. Sci.* **33** (suppl.), A127 (1998).
10. L. A. Haskin and P. H. Warren, in *Lunar Sourcebook,* G. H. Heiken, D. T. Vaniman, B. M. French, Eds. (Cambridge Univ. Press, New York, 1991), pp. 367–474, figure 8.3. The inverse correlation between FeO and CaO is principally due to variations in the abundance of anorthite, a Ca-rich and Fe-poor plagioclase. At higher FeO contents where the correlation flattens, the rocks are typically mare basalts, which contain less anorthite but more calcic pyroxenes.
11. R. Lingenfelter, E. H. Canfield, V. E. Hampel, *Earth Planet. Sci. Lett.* **16**, 355 (1972).
12. W. C. Feldman, R. C. Reedy, D. S. McKay, *Geophys. Res. Lett.* **18**, 2157 (1991).
13. D. J. Lawrence *et al.*, *Science* **281**, 1484 (1998).
14. *Note added in proof*: The fast neutron data suggest that the CSR FeO abundances in South Pole–Aitken basin may be overestimated. If so, then it is likely that Gd and Sm abundances are higher there than we have estimated, and the basin is richer in incompatible elements than we have suggested.

15. This research was partially supported by NASA through a subcontract from Lockheed-Martin Corporation. We thank R. Reedy and D. Vaniman for discussions, P. Spudis and another referee for helpful and thorough reviews, and D. Thomsen for maps of lunar surface features. This work was performed under the auspices of the U.S. Department of Energy.

13 July 1998; accepted 7 August 1998

Fluxes of Fast and Epithermal Neutrons from Lunar Prospector: Evidence for Water Ice at the Lunar Poles

W. C. Feldman,* S. Maurice, A. B. Binder, B. L. Barraclough, R. C. Elphic, D. J. Lawrence

Maps of epithermal- and fast-neutron fluxes measured by Lunar Prospector were used to search for deposits enriched in hydrogen at both lunar poles. Depressions in epithermal fluxes were observed close to permanently shaded areas at both poles. The peak depression at the North Pole is 4.6 percent below the average epithermal flux intensity at lower latitudes, and that at the South Pole is 3.0 percent below the low-latitude average. No measurable depression in fast neutrons is seen at either pole. These data are consistent with deposits of hydrogen in the form of water ice that are covered by as much as 40 centimeters of desiccated regolith within permanently shaded craters near both poles.

The moon is depleted in all volatile elements compared with Earth (*1*). However, water was brought to the moon by comets and asteroids and was formed by the reduction of FeO in lunar materials by solar wind hydrogen, and some juvenile water may have been released from the lunar interior over billions of years (*2*, *3*). Studies of the transport of such water over the lunar surface after its release indicate that 20 to 50% should be retained as frozen water ice within permanently shaded craters near both poles (*2–6*). However, losses due to meteoritic bombardment (*3*) and erosion due to particle sputtering (*7*), or photodissociation by interstellar hydrogen Lyman-α (*8*), may exceed the accretion rate preventing the development and retention of permanent ice deposits at the poles.

W. C. Feldman, B. L. Barraclough, R. C. Elphic, D. J. Lawrence, Los Alamos National Laboratory, MS D-466, Los Alamos, NM 87545, USA. S. Maurice, Observatoire Midi-Pyrenees, 14 avenue Edouard Belin, 31400 Toulouse, France. A. B. Binder, Lunar Research Institute, 1180 Sunrise Drive, Gilroy, CA 95020, USA.

*To whom correspondence should be addressed. E-mail: wfeldman@lanl.gov

The interpretation of anomalously large intensities of same-sense polarized radar echoes that are localized to permanently shaded craters near the poles of Mercury (*9–11*) as caused by deposits of nearly pure water ice suggests that similar deposits should also exist on the moon. Although a report of a possible detection of water ice on the moon with Clementine data (*12*) supports this suggestion, it is not universally accepted (*13*, *14*). We address the question of lunar water ice using epithermal- and fast-neutron data measured using the Lunar Prospector (LP) neutron spectrometer (NS).

Expected signature of H. A unique identification of chemical species enriched in hydrogen and a characterization of their spatial distribution are possible through measurement of neutron flux spectra (*15*, *16*). The magnitude of this effect at 100-km altitude is illustrated with simulated neutron flux spectra (Fig. 1). The different curves give neutron lethargy, $L(E)$, as a function of energy, E, for ferroan-anorthosite (FAN, a major type of soil or regolith in the lunar highlands) containing various admixtures of H_2O (*17*). There are three general energy ranges that